Integration of the Vegetation Phenology Module Improves Ecohydrological Simulation by the SWAT-Carbon Model

Mingwei Li[1], Shouzhi Chen[1], Fanghua Hao[1], Nan Wang[1], Zhaofei Wu[1], Yue Xu[2], Jing Zhang[1], Yongqiang Zhang[3], Yongshuo H. Fu[1]

[1]College of Water Sciences, Beijing Normal University, Beijing 100875, China
[2]College of Urban and Environmental Sciences, Central China Normal University, Wuhan 430079, China
[3]Key Laboratory of Water Cycle and Related Land Surface Processes, Institute of Geographic Sciences and Natural Resources Research, Chinese Academy of Sciences, Beijing 100101, China

Correspondence to: Yongshuo H. Fu (yfu@bnu.edu.cn)

Abstract. Vegetation phenology and hydrological cycles are closely interacted from leaf and species levels to watershed and global scales. As one of the most sensitive biological indicators of climate change, plant phenology is essential to be simulated accurately in hydrological models. Despite the Soil and Water Assessment Tool (SWAT) has been widely used for estimating hydrological cycles, its lack of integration with the phenology module has led to substantial uncertainties. In this study, we developed a process-based vegetation phenology module and coupled it with the SWAT-Carbon model to investigate the effects of vegetation dynamics on runoff in the upper reaches of Jinsha River watershed in China. The modified SWAT-Carbon model showed reasonable performance in phenology simulation, with root mean square error (RMSE) of 9.89 days for the start-of-season (SOS) and 7.51 days for the end-of-season (EOS). Simulations of both vegetation dynamics and runoff were also substantially improved compared to the original model. Specifically, the simulation of leaf area index significantly improved with the coefficient of determination (R^2) ~~increased~~ increasing by 0.62, the Nash–Sutcliffe efficiency (NSE) ~~increased~~ increasing by 2.45, and the absolute percent bias (PBIAS) ~~decreased~~ decreasing by 69.0 % on average. Additionally, daily runoff simulation also showed ~~notably~~notable improvement, particularly noticeable in June and October, with R^2 rising by 0.22 and NSE rising by 0.43 on average. Our findings highlight the importance of integrating vegetation phenology into hydrological models to enhance modeling performance.

1 Introduction

Vegetation plays a crucial role as a link between the land and the atmosphere through its influence on ~~the processes of the~~ carbon, water, and energy cycles (Bonan, 2008; Zhou et al., 2023). Plant phenology is one of the most sensitive bioindicators of climate change (IPCC, 2021; Fu et al., 2015; Vitasse et al., 2022)~~,~~ and closely ~~interacting~~ interacts with the hydrological cycles (Chen et al., 2022a; Hwang et al., 2014; Kim et al., 2018). Therefore, vegetation phenological processes must be accurately simulated ~~accurately~~ in hydrological models. The Soil and Water Assessment Tool (SWAT) has been widely used to model ~~watershed~~ hydrological ~~characteristics~~ processes in watersheds (Bhatta et al., 2019; Tian et al., 2020). However, the

performance of its vegetation module and its simulation of vegetation phenology remains poor, resulting in large uncertainties in the simulation of hydrological processes (Chen et al., 2023). To improve predictions of ecohydrological processes under future climate change conditions, it is essential to modify the vegetation module by considering vegetation phenology.

In recent decades, climate change has substantially shifted vegetation phenology, with an advance in the start-of-season (SOS) (Fu et al., 2014) and a delay in the end-of-season (EOS) (Piao et al., 2019). This has extended contributed to the extension of the growing season by 2–10 days per decade (Zhao et al., 2015; Garonna et al., 2016; Shen et al., 2022), closely interacting with hydrological processes from leaf, and species levels to watershed and global scales (Chen et al., 2022b). At the leaf scale, earlier spring leaf-out would enhance the transpiration and increase the water requirement of plants, resulting in increased greater water flux from the soil to the atmosphere. At the watershed scale, the extension of the vegetation growing season would reduce runoff through increased evapotranspiration (ET) (Gaertner et al., 2019; Geng et al., 2020; Kim et al., 2018). Shifting Shifts in vegetation phenology affects both the magnitude and the timing of hydrological processes (Creed et al., 2015; Hwang et al., 2023). Therefore, developing a hydrological model capable of characterizing vegetation phenology is essential for a comprehensive understanding of hydrological processes.

The SWAT model has been extensively used to assess the impact of climate change on water processes across a variety of watershed scales. The updated SWAT-Carbon model was developed to improve performance in terms enhance the simulation of terrestrial carbon and water cycles (Mukundan et al., 2023; Zhang et al., 2013). As in the original versionSWAT, SWAT-Carbon employs a simplified version of the Environmental Policy Impact Climate (EPIC) vegetation growth module (Arnold et al., 1998), which determines SOS and EOS based on a daylength threshold calculated as a function of latitude. However, phenological processes are complex, determined not only by daylength, but also by temperature and precipitation (Piao et al., 2015; Wu et al., 2023; Peñuelas et al., 2004). For example, temperature is regarded as the dominant driver of spring phenology, with spring warming largely advancing leaf-out dates by meeting the forcing requirement earlier (Ge et al., 2015; Fu et al., 2018). However, winter warming-induced reductions in chilling accumulation would increase the forcing requirement and delay the leaf-out dates (Fu et al., 2015; Wu et al., 2023). Therefore, the EPIC module cannotfails to capture the real phenological processes (Ma et al., 2019), and making it urgent to coupling couple a specific phenology module with the SWAT-Carbon model is urgently needed to accurately simulate hydrological processes accurately.

The Tibetan Plateau has experienced seriously climate change, greatly influencing vegetation dynamics and regional water cycles (Shen et al., 2022; Li et al., 2022). The upper reaches of the Jinsha River watershed, originating from the Tibetan Plateau and forming the upper reach of Yangtze River, is recognized as one of the ecologically fragile regions in China. In recent years, the upper reaches of the Jinsha River watershed experienced significant climate change, greatly influencing vegetation dynamics and regional water cycles (Wu et al., 2020; Jiang et al., 2024; Li et al., 2022). Enhancing our

understanding and simulation of ecohydrological processes in the upper reaches of the Jinsha River watershed is critical for securing water resources and maintaining ecological stability. In this study, ~~utilizing a typical watershed in the Tibetan Plateau, upper reaches of the Jinsha River watershed,~~ we first developed a process-based vegetation phenology module for the upper reaches of the Jinsha River watershed, which consist~~sed~~ of spring and autumn phenology models that consider~~s~~ both temperature and photoperiod. Subsequently, we coupled this module ~~into~~ with the SWAT-Carbon model. The objectives of our study are as follows: 1) to develop a process-based vegetation phenology module and integrate it into the SWAT-Carbon model; 2) to elucidate the effects of vegetation phenology and climate change on watershed ecohydrological processes; and 3) to forecast future shifts in runoff under different emission scenarios using the modified SWAT-Carbon model.

2 Materials and Methods

2.1 Study Area

Our study focused on the upper reaches of the Jinsha River watershed in China, ~~and the Jinsha River is~~ located in the upper reach of the Yangtze River (Figure 1a). The elevation difference of the upper Jinsha River watershed is 4,773 m (Figure 1b), and the drainage area ~~is~~ covers 216,440 km^2. The multiyear mean temperature ~~is~~ was approximately -2.56 ± 4.11 ℃, and the multiyear mean annual precipitation ~~is~~ was approximately 467 ± 135 mm from 1982 to 2018. Influenced by monsoons, precipitation is mainly observed during June–September, accounting for over 75 % of the annual total, with peak precipitation ~~typically~~mostly occurring in July. The land use types in the study area ~~showed minimal~~ changed little during 2007–2014, with grassland (61.4 %) and forest (14.6 %) representing the dominant vegetation types (Figure 1c). Grassland areas are primarily distributed in the upstream region of the basin, whereas forests are prevalent in the downstream area.

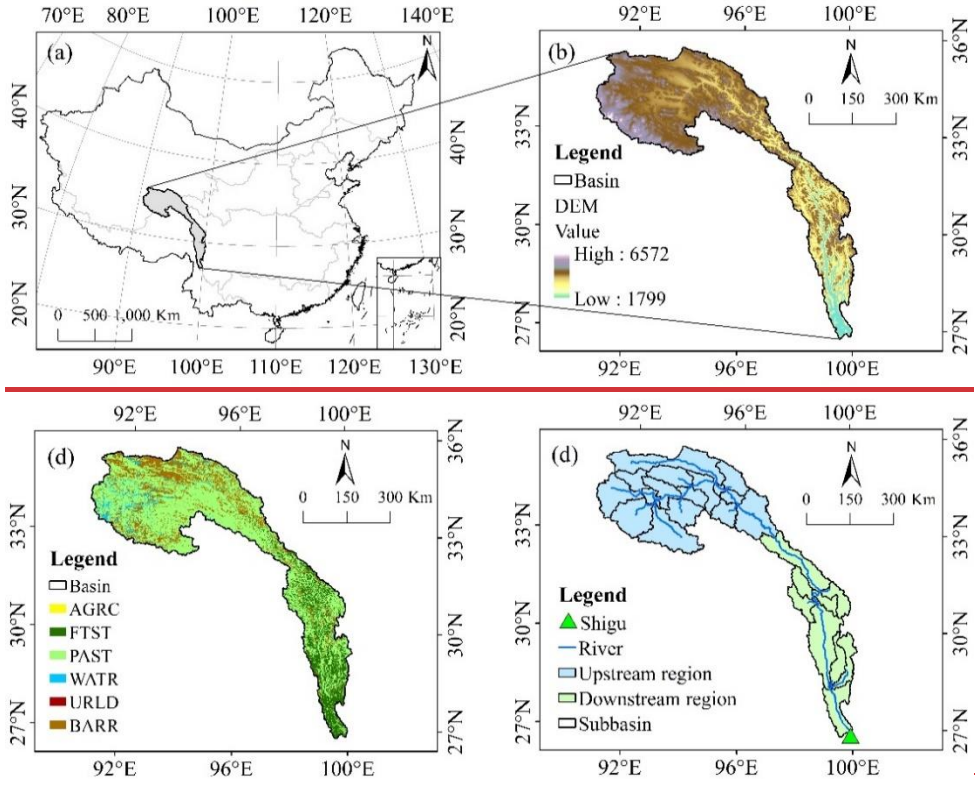
(a)
70°E
80°E
100°E
120°E
140°E
40°N
30°N
20°N
N
0 500 1,000 Km
90°E
100°E
110°E
120°E
130°E
(b)
92°E
96°E
100°E
36°N
33°N
30°N
27°N
N
0 150 300 Km
Legend
Basin
DEM
Value
High : 6572
Low : 1799
(d)
Legend
Basin
AGRC
FTST
PAST
WATR
URLD
BARR
(d)
Legend
Shigu
River
Upstream region
Downstream region
Subbasin

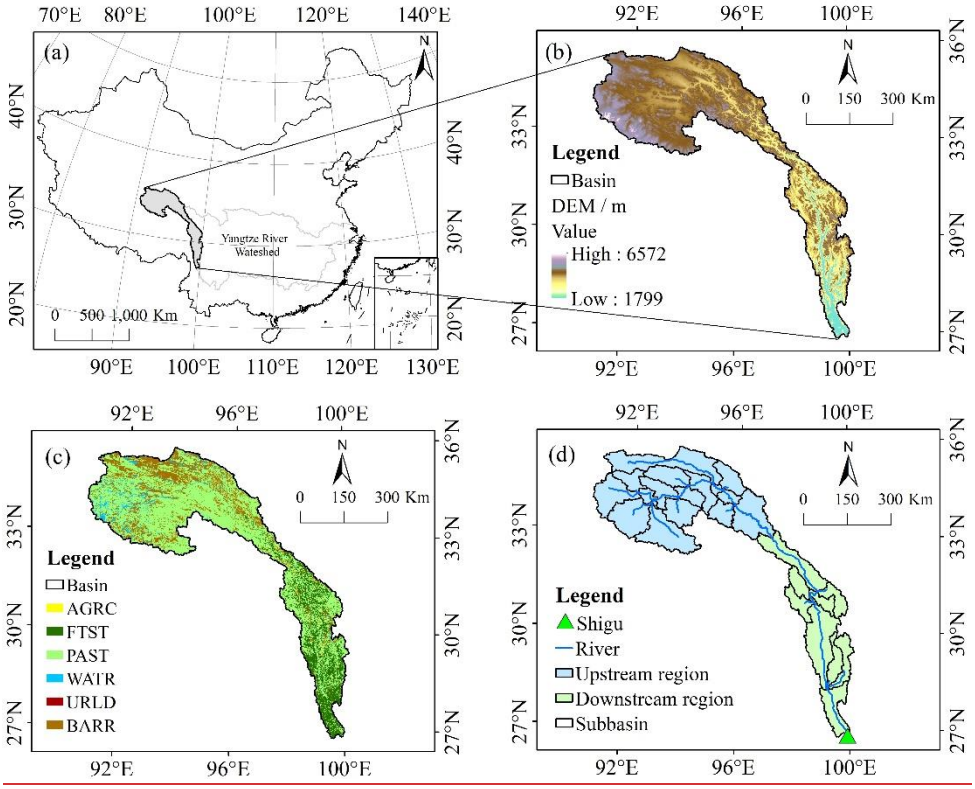

Figure 1: Study area. (a) Location of the upper Jinsha River watershed, (b) digital elevation model (DEM), (c) distribution of land use types (AGRC-farmland, FRST-forest, PAST-grassland, WATR-water, URLD- residential area, BARR-unused land), and (d) division of subbasins and the location of the Shigu hydrological gauging station.

2.2 Dataset

The sources of the datasets used for phenology models and the SWAT-Carbon model are listed in Table 1.

2.2.1 Digital Elevation Model (DEM), Land Use, and Soil Data

The watershed and river network of the study area were delineated using a digital elevation model (DEM) with 90-m resolution (Figure 1b) in ArcSWAT2012 (https://swat.tamu.edu/). The watershed was first subdivided into 28 subbasins (Figure 1d) ~~using~~ based on topographic characteristics~~,~~ and then discretized into 1,922 hydrologic response units (HRUs) based on land use, soil data, and slope characteristics.

We extracted land use data with 1-km spatial resolution from the Resources and Environmental Sciences and Data Center, Institute of Geographic Sciences and Natural Resources Research, Chinese Academy of Sciences (https://www.resdc.cn/). This ~~extracted~~ data w~~as~~ere reclassified to match the land use classes for HRU delineation in the SWAT-Carbon model (Figure 1c). There were six classes of land use identified in the watershed: farmland (ARGC), forest (FRST), grassland (PAST), water (WATR), residential area (URLD), and unused land (BARR).

The soil map of the upper reaches of the Jinsha River watershed was obtained from the Food and Agriculture Organization of the United Nations (http://www.fao.org). We used the Soil Water Atmosphere Plant model (SWAP: http://hydrolab.arsusda.gov/soilwater) to develop the database of soil properties for the ~~studied~~ watershed.

2.2.2 Climate Data and Runoff

~~Because of the limited distribution of meteorological stations in the study area, g~~Gridded climate data were ~~used~~ processed as observed values to force both the original and the modified SWAT-Carbon models, considering of the limited distribution of meteorological stations. We used daily meteorological data from 1982 to 2018 with 0.1° spatial resolution, extracted from the China Meteorological Forcing Dataset (CMFD), which included precipitation, temperature, relative humidity, wind speed, and solar radiation (He et al., 2020). This dataset was developed by the Institute of Tibetan Plateau Research under the Chinese Academy of Sciences, and it represents the optimal combination of ~~in~~ in-situ observations, satellite ~~retrials~~ retrievals, and meteorological reanalysis.

CMIP6 outputs were used to predict vegetation phenology and future runoff. We selected four CMIP6 models, i.e., CanESM5, FGOALS-g3, MPI-ESM1-2-HR, and MRI-ESM2-0, which were commonly used in studies of the Yangtze River (Zhang et al., 2023; He et al., 2024) ~~under three emission scenarios (SSP1-2.6, SSP2-4.5 and SSP5-8.5), to predict vegetation phenology and future runoff~~. The ~~Daily~~daily time series of mean temperature, maximum temperature, minimum temperature, and precipitation under three emission scenarios (SSP1-2.6, SSP2-4.5, and SSP5-8.5) were acquired from the CMIP6 website (https://esgf-node.llnl.gov/search/cmip6/). CMIP6 data are biased in local areas (Stevens and Bony, 2013), ~~and therefore~~making it ~~is~~ necessary to correct ~~those~~ these errors. First, we interpolated the CMIP6 data to 0.1° spatial resolution using linear interpolation. Then, the CMFD was employed as the reference to correct the bias in CMIP6 models using the empirical mapping technique (Gudmundsson et al., 2012; Wilcke et al., 2013). Daily empirical cumulative distribution functions for the calibration period were produced using a moving window of ±15 days (Thrasher et al., 2012).

Daily runoff data (2007–2014) of the Shigu hydrological gauging station, located at the upper reaches of Jinsha River watershed outlet, were obtained from the Chinese Hydrological Data Yearbook.

2.2.3 Vegetation Data

We obtained the Global Inventory Modeling and Mapping Studies third generation normalized difference vegetation index (GIMMS3g NDVI) dataset from the Ecological Forecasting Lab (https://data.tpdc.ac.cn/en/data/9775f2b4-7370-4e5e-a537-3482c9a83d88/) for 1982–2020 (spatial resolution: 1/12°, temporal resolution: every 15 d).

Leaf area index (LAI) data from 1982 to 2018 was acquired from the Global Land Surface Satellite (GLASS) product with 0.05° spatial resolution and an eight-day temporal interval (http://glass-product.bnu.edu.cn). LAI time series for forest and

grassland areas were obtained through area-weighted averaging of FRST and PAST grid values within the studied watershed (Strauch and Volk, 2013; Zhang et al., 2020).

Table 1: Details of the data used in this study.

Data	Source	Characteristics
Digital elevation model (DEM)	Geospatial Data Cloud (https://www.gscloud.cn/)	SRTMDEM 90M
Land use types	Center for Resources and Environmental Sciences and Data (https://www.resdc.cn/)	~~1~~ 1-km spatial resolution
Soil map	Food and Agriculture Organization of the United Nations (http://www.fao.org)	Harmonized World Soil Database v 1.2
Observed meteorological data	China Meteorological Forcing Dataset (https://data.tpdc.ac.cn/home)	daily, 0.1° spatial resolution
Observed runoff	Chinese Hydrological Data Yearbook	Shigu hydrological gauging station, daily
Normalized difference vegetation index (NDVI)	Global Inventory Modeling and Mapping Studies third generation ($GIMMS_{3g}$) (https://data.tpdc.ac.cn/en/data/9775f2b4-7370-4e5e-a537-3482c9a83d88/)	15 d, 1/12° spatial resolution
Leaf area index ~~data~~ (LAI)	Global Land Surface Satellite (GLASS) product (http://glass-product.bnu.edu.cn).	8 d, 0.05° spatial resolution

2.3 SWAT-Carbon Model Modification

The SWAT model is a comprehensive, process-oriented, and physically based~~/process based~~ semi-distributed hydrological model (Neitsch et al., 2011). The SWAT-Carbon model (https://sites.google.com/view/swat-carbon/home), as an updated version~~vision~~, is developed to enhance the simulation of terrestrial carbon cycles. However, the SWAT-Carbon model still performs poorly in estimating vegetation dynamics (e.g., phenology and LAI). The current SWAT-Carbon model uses daylength thresholds, that are determined only by latitude, to simulate the onset and the end of vegetation dormancy. This approach fails to accurately capture vegetation dynamics as it largely ignores the effects of other important environmental factors (i.e., temperature) (Chen et al., 2023). ~~More realistic~~ Incorporating accurate phenology ~~data~~ information could enhance the ~~performance~~ simulation of LAI ~~simulation~~, ~~which would further improve~~ thereby improving the accuracy of runoff simulated by the hydrological model. The UniChill model and the DM model, which account for the response of phenology to various environmental variations, have been widely used to simulate spring and autumn phenology (Roberts et al., 2015; Yang et al., 2012). Therefore, we ~~developed a novel method to enhance~~modified the SWAT-Carbon model by integrating ~~a~~ the process-based vegetation phenology module ~~into it~~. This phenology module consists of two phenology models: the UniChill model for simulating SOS and the DM model for simulating EOS. These phenology models provide

dynamic simulations of plant phenology to replace the ~~exact~~ fixed dates of the SOS and EOS in the SWAT-Carbon model without the need for ~~any~~ adjusting management ~~settings in the~~ operations ~~schedule~~. Subsequently, we set the heat accumulation calculated between dynamic phenology dates, instead of the default constant, as the annual heat requirement for vegetation growth. This dynamic heat requirement was then used to calculate daily variations in LAI.

The UniChill model, proposed by Chuine (2000), hypothesizes that spring phenology is regulated both by chilling temperatures and by forcing temperatures during the dormancy period. Because of the specific ~~certain~~ range of chilling and forcing temperatures, we added temperature conditions when calculating the state of the chilling and forcing phases (Fu et al., 2012). The chilling phase starts at the onset of dormancy (t_0, fixed to 1 September), and is active on days with mean temperature between -5 and 10 ℃. The rate of chilling can be expressed as follows:

$$R_C = \begin{cases} \dfrac{1}{1+e^{C_a(x-C_c)^2+C_b(x-C_c)}} & if\ -5 \le x \le 10 \\ 0 & if\ x > 10\ or\ x < -5 \end{cases} \quad (1)$$

where x is the daily mean air temperature, and C_a, C_b, and C_c are chilling rate parameters.

The chilling phase ends with the onset of quiescence (t_1), which occurs ~~is~~ when the state of chilling (S_C; Eq. 2) reaches the critical state of chilling (Eq. 3):

$$S_C = \sum_{t_0}^{t} R_C(x_t) \quad (2)$$

$$t = t_1 \quad if \quad S_C > C^* \quad (3)$$

The forcing phase begins at t_1, and ~~it~~ is active on days with mean temperature is above 0 ℃.

$$R_F = \begin{cases} \dfrac{1}{1+e^{F_b(x-F_c)}} & if\ x > 0 \\ 0 & if\ x \le 0 \end{cases} \quad (4)$$

where F_b and C_c are forcing rate parameters.

The forcing phase ends with the occurrence of SOS (t_2), which occurs ~~is~~ when the state of forcing (S_F; Eq. 5) reaches the critical state of forcing (Eq. 6):

$$S_F = \sum_{t_1}^{t} R_F(x_t) \tag{5}$$

$$t = t_2 \quad if \quad S_F > F^* \tag{6}$$

The DM model (Delpierre et al., 2009) is based on the assumption that leaf senescence is driven both by the photoperiod and by low temperatures. This model represents the progress of senescence processes using a coloring state (S_{sen}) for each day (d), which is the accumulation of the daily rate of senescence (R_{sen}). Senescence starts on the date (D_{start}) when the photoperiod is shorter than a specific~~certain~~ threshold (P_{start}), and the EOS is recognized as when S_{sen} exceeds~~is larger than~~ the threshold value Y_{crit}. The functions expressed in the process are as follows:

$$if \ P(d) < P_{start} \begin{cases} if & T(d) < T_b \quad R_{sen}(d) = [T_b - T(d)]^x \times f[P(d)]^y \\ if & T(d) \geq T_b \quad R_{sen}(d) = 0 \end{cases} \tag{7}$$

$$if \ \begin{cases} P(d) \geq P_{start} & S_{sen}(d) = 0 \\ P(d) < P_{start} & S_{sen}(d) = S_{sen}(d-1) + R_{sen}(d) \end{cases} \tag{8}$$

$$f[P(d)] = \frac{P(d)}{P_{strat}} \quad \text{or} \quad f[P(d)] = 1 - \frac{P(d)}{P_{strat}} \tag{9}$$

where $P(d)$ is the photoperiod on a given day d, $T(d)$ is the daily mean temperature (℃), and Tb is the critical temperature below which senescence processes are effective (℃).

We calibrated and validated the two phenology models using all pixel-year SOS and EOS data extracted from the GIMMS3g NDVI dataset during 1982–2018. Five phenological extraction methods (i.e., the HANTS-Maximum, Spline-Midpoint, Gaussian-Midpoint, Timesat-SG, and Polyfit-Maximum methods) were applied to obtain the mean phenological index value, reducing the uncertainty caused by the use of only a single method (Fu et al., 2021). To match the spatial resolution of gridded meteorological data, the SOS and EOS data were resampled to 0.1° spatial resolution, and outliers were removed using the interquartile range method (Cui et al., 2017). We optimized parameters of the UniChill model (i.e., C_a, C_b, C_c, F_b, C_c, C^*, *and* F^*) and the DM model (i.e., P_{start}, T_b, x, y, *and* Y_{crit}) for each valid pixel in upper reaches of the Jinsha River watershed, minimizing the root mean square error (RMSE) through particle swarm optimization. Phenology data from odd-numbered years were utilized for parameter optimization, and even-numbered years were used for validation.

The warming-up, calibration, and validation periods for the original and modified SWAT-Carbon models were set at 2005–2006, 2007–2011, and 2012–2014, respectively. The calibration of the modified SWAT-Carbon model involved the following two steps, whereas that of the original SWAT-Carbon model ~~only~~ employed only the second step. 1) We optimized the ~~8~~ eight parameters (Table S1) that control the shape, magnitude, and temporal dynamics of the LAI for forest and grassland through particle swarm optimization, to align the simulated LAI curves with the observed dynamic LAI. ~~10~~

Ten particles with different initial velocities were generated through the Latin hypercube sampling method. The Nash–Sutcliffe efficiency (NSE) was used as the objective function to continuously update the parameters. Optimal parameter sets were determined when the objective function remained unchanged after ~~10~~ ten iterations. 2) We adjusted those parameters that control the hydrological processes using SWAT-CUP 2019 (https://swat.tamu.edu/software/swat-cup/) (Abbaspour, 2008). The Sequential Uncertainty Fitting (Sufi-2) algorithm in SWAT-CUP was used for sensitivity analysis, uncertainty analysis, and parameter calibration (Arnold et al., 2012). Overall, 18 parameters (Table S2) were used for model calibration. These parameters were derived by combining the 14 most sensitive parameters selected from the pool of 22 parameters for each original and modified model.

2.4 Model Evaluation

The widely used coefficient of determination (R^2), NSE, and percent bias (PBIAS) were selected as metrics to evaluate the performance of the model in simulating ~~the~~ LAI and runoff in our study area (Moriasi et al., 2007):

$$R^2 = \frac{\left(\sum_{i=1}^{n}\left(O_i-\overline{O}\right)\left(P_i-\overline{P}\right)\right)^2}{\sum_{i=1}^{n}\left(O_i-\overline{O}\right)^2\sum_{i=1}^{n}\left(P_i-\overline{P}\right)^2} \quad (10)$$

$$NSE = 1-\frac{\sum_{i=1}^{n}\left(O_i-P_i\right)^2}{\sum_{i=1}^{n}\left(O_i-\overline{O}\right)^2} \quad (11)$$

$$PBIAS = \frac{\overline{P}-\overline{O}}{\overline{O}}\times 100\% \quad (12)$$

where n is the number of observations; O_i and P_i are the observed and simulated values, respectively, at time i; and $\overline{O}$ and $\overline{P}$ represent the average of the observed and simulated values, respectively.

3 Results

3.1 Spatiotemporal Variations in Climate and Vegetation Phenology

There is notable spatiotemporal heterogeneity in the multiyear mean annual temperature and accumulated precipitation across the upper reaches of the Jinsha River watershed (Figure 2a and 2b). The mean annual temperature exhibits a gradual increase from the upstream to the downstream areas. The annual accumulated precipitation is higher in the downstream region ~~compared to~~than in the upstream. In addition, the mean annual temperature and accumulated precipitation showed clear temporal trends during 1982-2018. The mean annual temperature significantly increased by 0.06 °C per year on

average. The annual accumulated precipitation across the entire watershed increased by 2.64 mm per year~~,—.~~ ~~however~~However, downstream regions exhibited a declining trend (Figure ~~Fig.~~2b). Over the past four decades, the upper reaches of the Jinsha River watershed ~~have~~ showed a “warming–wetting” trend in the upstream area and a “warming–drying” trend in some downstream areas.

During 1982–2018, the multiyear mean SOS and EOS in the upper reaches of the Jinsha River watershed were 164 ± 12~~.16~~ and 298 ± ~~10.56~~11, (Day of year, DoY), respectively (Figure 2c and 2d). The mean SOS initiated in early May upstream and early July downstream. The mean EOS occurred in early October upstream, one month earlier than downstream. The SOS advanced in 60.5% of the study area over the past four decades, primarily in the middle and upper reaches of the watershed (-0.05 ± 0.13 days per year), while being delayed by 0.09 ± 0.30 days per year in the downstream area. During the study period, the EOS was delayed by 0.08 ± 0.27 days per year in the downstream area but advanced by -0.03 ± 0.14 days per year in the upstream area. This spatiotemporal heterogeneity of vegetation phenology further highlights the importance of incorporating vegetation dynamics into hydrological models.

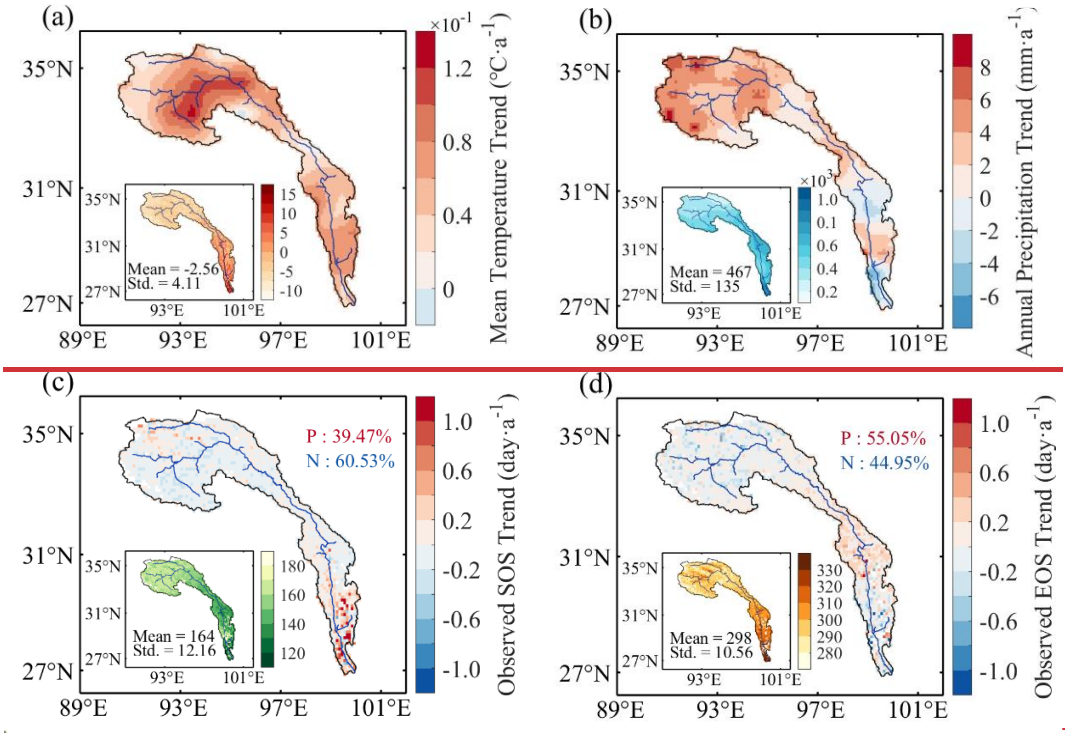

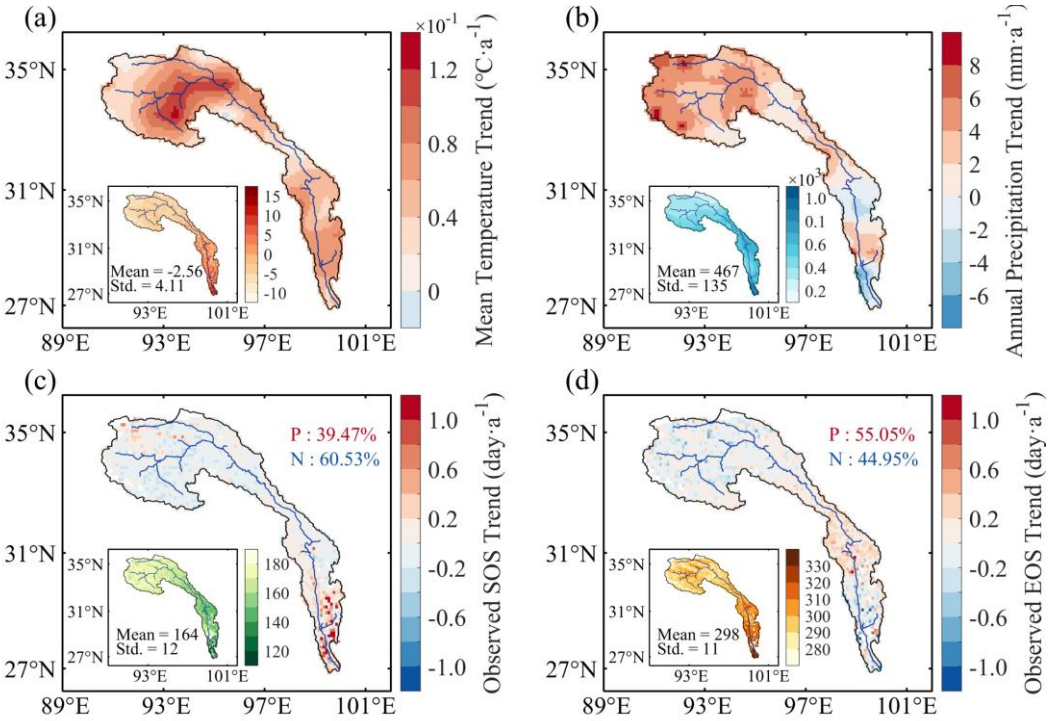

Figure 2: Spatial and temporal variations of climatic variables and vegetation phenology during 1982–2018. Temporal variations of mean annual temperature (a), accumulated annual precipitation (b), start-of-season (SOS, c), and end-of-season (EOS, d). The inner plot of each subfigure depicts the spatial pattern of the multi-year means of each variable. P, percentage of pixels showing a positive trend, indicates increased temperature and precipitation, or delayed SOS and EOS; N, percentage of pixels showing a negative trend, indicates decreased temperature and precipitation, or advanced SOS and EOS.

3.2 Performance of Phenology Module and Modified SWAT-Carbon Model

The mean RMSE for the spring and autumn phenology models ~~is~~ are 9.89 and 7.51 days, with calibration and validation RMSEs of 8.71 and 10.82 days for SOS, and 7.03 and 7.77 days for EOS, respectively (Fig.3a and b). Within the study area, 67.1% and 85.8% of pixels exhibited an RMSE of less than 10 days for SOS and EOS, respectively. The correlation coefficients between observed and simulated SOS and EOS are 0.54 and 0.63, respectively.

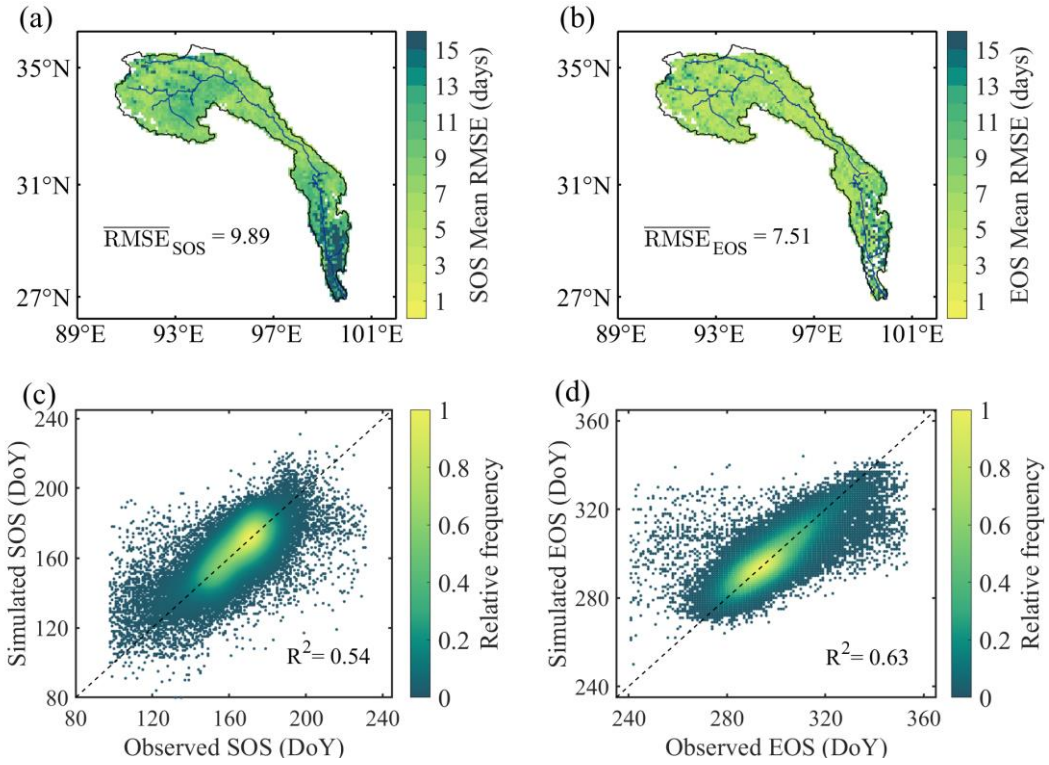

Figure 3: Performance of phenology module. Spatial patterns of the RMSE for start-of-season (SOS, a) and end-of-season (EOS, b). Scatter plots depicting the relationship between simulated and observed start-of-season (SOS, c) and end-of-season (EOS, d). The overlined RMSE represents the average RMSE. The colored points on the scatter plots represent kernel density, with lighter colors indicating a higher density distribution. The dashed line represents the 1:1 ratio line.

In the modified SWAT-Carbon model, the fixed phenology dates were replaced by the outcomes of phenology module, and the simulated LAI before the start of the growing season was changed to a non-zero value for both ~~the~~ forest and grassland~~, .~~ and~~After these modifications,~~ the calibrated and validated LAI growth curves largely improved compared to the original model (Figure 4a and 4b, Table 2). Specifically, the average R^2 and NSE values improved from 0.31 and -1.42 to 0.79 and 0.78 for forest, and from 0.13 and -1.84 to 0.88 and 0.87 for grassland~~ on average~~, respectively. Additionally, the absolute PBIAS decreased by 41.0% for forest and 97.0% for grassland. To further exclude the impact of non-growing season LAI, we also adjusted the non-growing season LAI to non-zero values in the original SWAT-Carbon model. The results indicated that, compared to the default settings, there were only slight improvements in the LAI growth curves in the original model (Figure S1). Specifically, the average NSE value improved from -1.42 to -0.29 for forest and from -1.84 to -0.70 for grassland, which is much smaller than NSE for LAI in the modified model. Furthermore, the average R^2 decreased by 0.17 for forest and by 0.01 for grassland, respectively.

Incorporating the phenology module into the SWAT-Carbon model enhanced the performance of runoff simulation. The modified SWAT-Carbon model produced runoff simulation~~s~~ with a 'very good' level of performance ($0.80 < R^2 \leq 1$ and 0.75

< NSE ≤ 1, Figure 4c and Table 2). Furthermore, the performance of runoff simulation ~~in various months exhibited~~ showed improvement in various months, particularly during the vegetation greening period (June), the senescence period (October), and the non-growing season (Table S3). Specifically, the R^2 and NSE values for runoff increased by 0.13 and 0.39 in June, respectively, by 0.30 and 0.46 in October. The NSE value for runoff from November of the previous year to May increased by 0.35.

Table 2: Evaluation indices of the original and modified SWAT-Carbon model in simulating LAI and runoff.

Variable	Evaluation indices	Calibration (2007–2011)		Validation (2012–2014)	
		Original	Modified	Original	Modified
LAI (forest)	R^2	0.28	0.77	0.33	0.80
	NSE	-1.47	0.76	-1.36	0.79
	PBIAS (%)	42.77	-1.50	41.75	1.12
LAI (grassland)	R^2	0.11	0.87	0.15	0.89
	NSE	-1.87	0.86	-1.80	0.88
	PBIAS (%)	97.47	0.65	97.15	-0.01
Runoff	R^2	0.93	0.95	0.89	0.92
	NSE	0.92	0.95	0.86	0.92
	PBIAS (%)	4.80	1.75	5.04	1.22

R^2, coefficient of determination; NSE, Nash–Sutcliffe efficiency; PBIAS, percent bias.

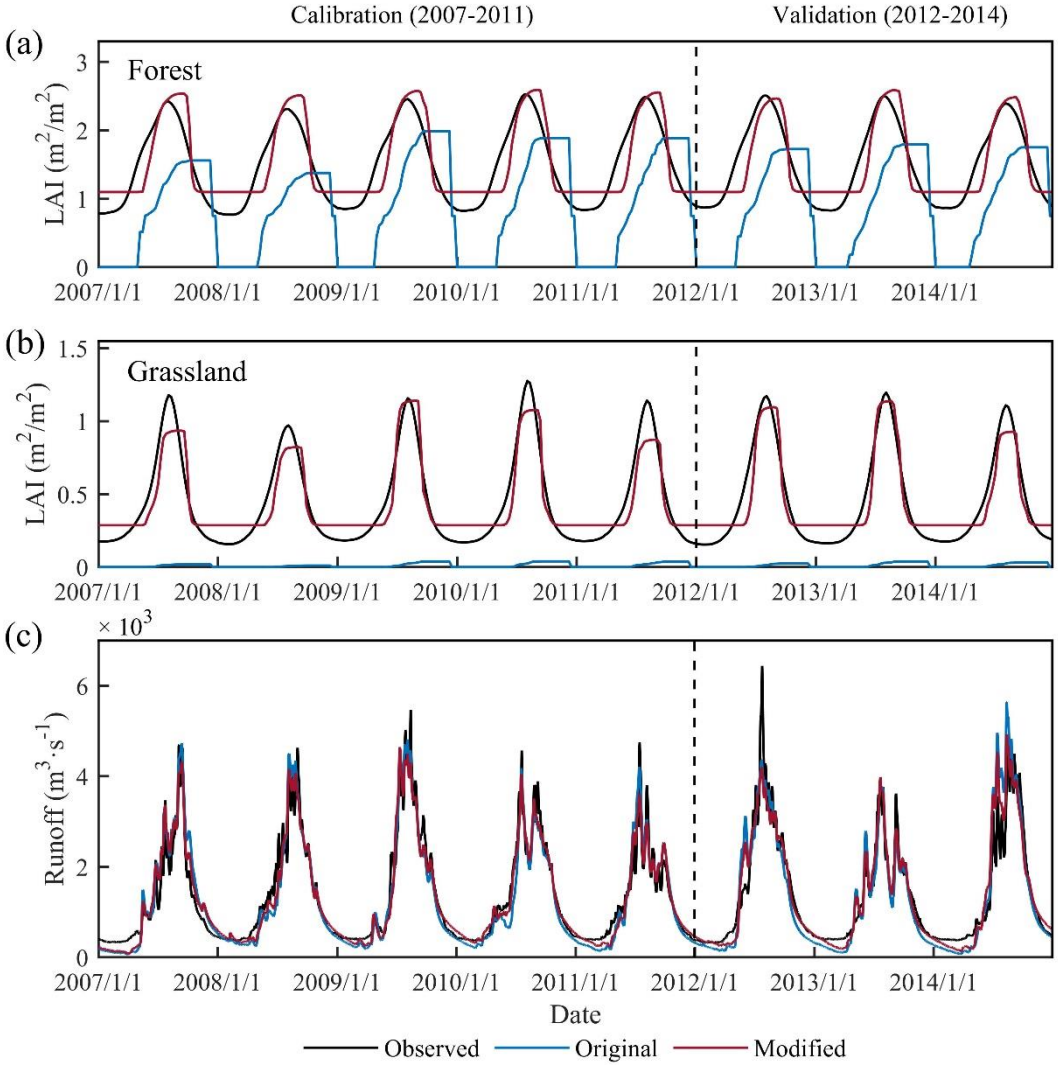

Figure 4: Temporal variability of the LAI and runoff during the calibration (2007–2011) and validation (2012–2014) periods. 8-d LAI time series observed by satellite and simulated by the original and modified SWAT-Carbon models for Forest (a) and grassland (b). Observed and simulated daily runoff by the original and modified SWAT-Carbon models (c).

3.3 Future Shifts in Vegetation Phenology and Runoff

The Unichill and DM phenology models were used to forecast future shifts in SOS and EOS during 2030–2100 under different emission scenarios. The SOS in the upper reaches of the Jinsha River watershed ~~is~~ was projected to advance under all scenarios (Figure 5a), with the most significant advancement observed under the high-emission scenario (0.49 days per year, $p < 0.0\text{~~0~~}1$). In addition, a delaying trend in EOS was observed under all scenarios (Figure 5b), with the largest delay occurring under the high-emission scenario (0.18 days per year, $p < 0.0\text{~~0~~}1$).

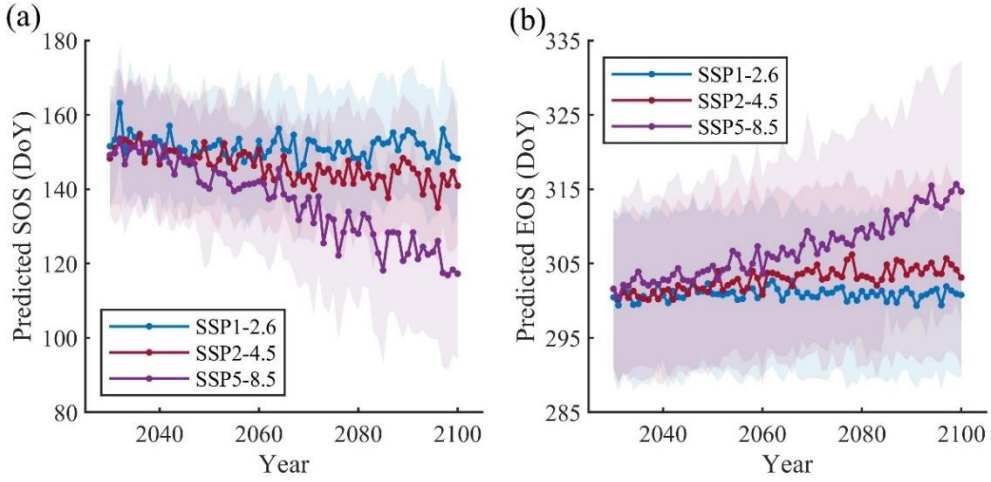

Figure 5: Projection of future spring and autumn phenology during 2030–2100. Future shifts in start-of season (SOS, a) and end-of-season (EOS, b) under three Shared Socioeconomic Pathway (SSP) scenarios based on the Coupled Model Intercomparison Project Phase 6 (CMIP6) multi-model ensemble. SSP1-2.6, SSP2-4.5 and SSP5-5.8 refer to low, moderate and high emissions, respectively. Colored lines and shading represent the mean and one standard deviation, across the four CMIP6 models under each emission scenario.

The runoff under SSP5-5.8 scenario exhibited greater fluctuation with a continuous increase from ~~2023~~ 2030 to 2100. Specifically, runoff ~~is~~ was projected to increase from approximately 1,437 $m^3 s^{-1}$ in 2030 to 3,638 $m^3 s^{-1}$ in 2100. However, the runoff under SSP1-2.6 and SSP2-4.5 scenarios is projected to initially increase and then stabilize after 2060 (Figure 6). The average runoff under SSP5-8.5 (2,459 $m^3 s^{-1}$) is greater than that under SSP1-2.6 (2,180 $m^3 s^{-1}$) and SSP2-4.5 (2,120 $m^3 s^{-1}$). ~~Results from the original SWAT-Carbon model underestimated the future increases in runoff compared to those produced by the modified SWAT-Carbon model~~ Results from the original SWAT-Carbon model showed a smaller increase in future runoff compared to those estimated by the modified SWAT-Carbon model (Figure ~~S1~~S2). Monthly total runoff outputs were obtained from CMIP6 models and aggregated to annual runoff from 2030 to 2100. We calculated the watershed-scale future runoff from CMIP6 using the area-weighted mean method and found that the future runoff from CMIP6 models was larger than that simulated by the modified SWAT-Carbon model (Figure S3).

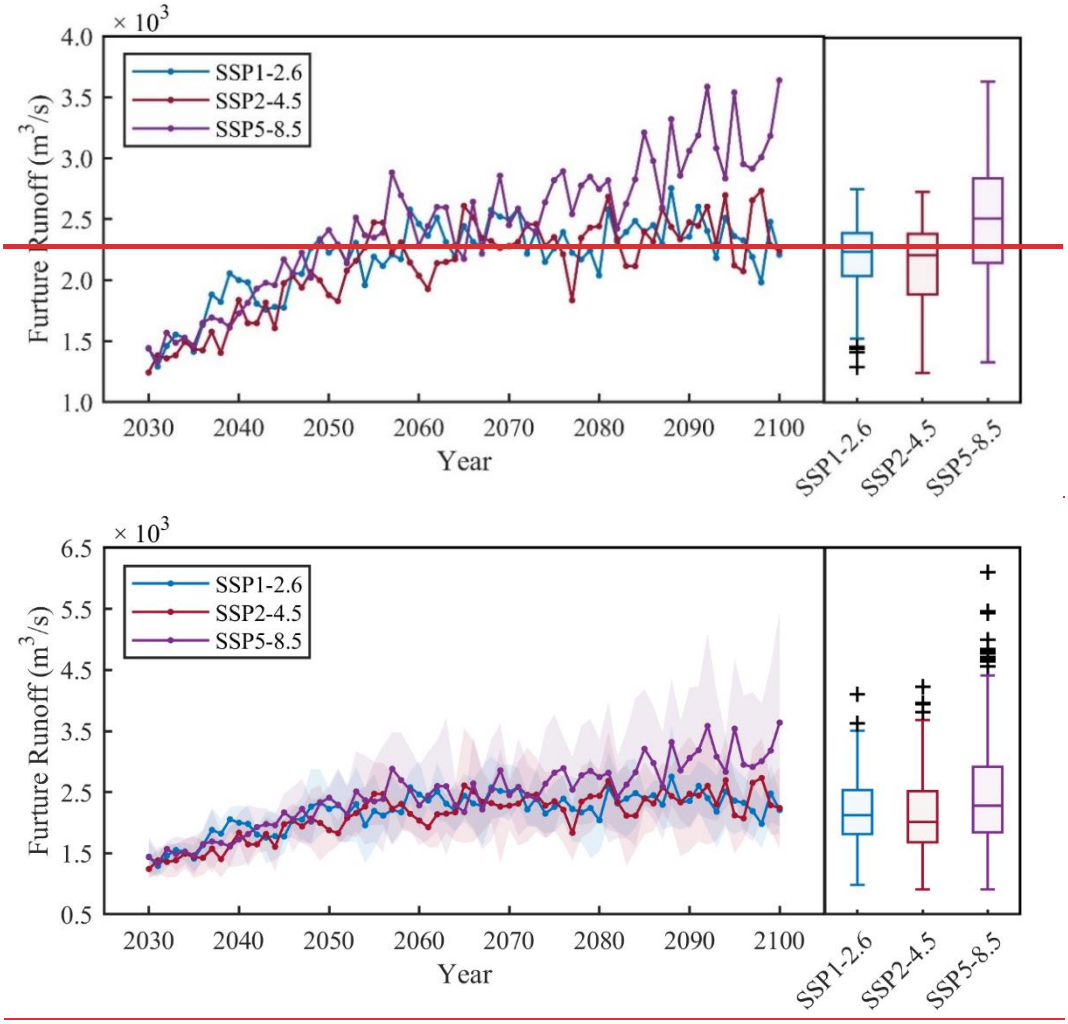

Figure 6: Projection of future runoff during 2030–2100 using the modified SWAT-Carbon model. ~~The right subplot represents the annual mean runoff. SSP1-2.6, SSP2-4.5 and SSP5-5.8 refer to low emission, moderate and high emissions, respectively, based on the Coupled Model Intercomparison Project Phase 6 (CMIP6) multi-model ensemble.~~Colored lines and shading in the right subplot represent the mean and one standard deviation across the four Coupled Model Intercomparison Project Phase 6 (CMIP6) models. The scenarios SSP1-2.6, SSP2-4.5, and SSP5-5.8 refer to low emission, moderate, and high emissions, respectively. The cross symbol represents the outlier.

4 Discussion

4.1 Improvement of Runoff Simulation by Modified Hydrological Model

Vegetation phenology has strong controls on seasonal and annual hydrological processes (Kim et al., 2018; Yang et al., 2023). ~~During the start and end of the growing season, rapid changes in vegetation physiological properties such as stomatal conductance and LAI influence the timing and amount of water resource allocation (Hwang et al., 2023; Zhang et al., 2021).~~

~~Various environmental factors (e.g., temperature, precipitation, and radiation) and vegetation types determine the start and the end of the growing season (Wu et al., 2021), and process based phenology models that incorporate different climatic factors have been well developed (Fu et al., 2020).~~ However, the vegetation phenology in most hydrological models, such as the SWAT-Carbon model, is based on simple thermal and daylength thresholds (Arnold et al., 1998). This approach results in large~~r~~ uncertainty in simulating vegetation dynamics and thereby in predicting hydrological processes~~ predictions~~, especially under climate change (Zhang et al., 2009; Wang et al., 2022; Ma et al., 2019). In this study, we integrated process-based spring and autumn phenology models into the SWAT-Carbon model, which substantially improved the simulation of vegetation dynamics and ecohydrological processes~~, especially during the months of spring and autumn vegetation growth~~. The simulation of the LAI curve, particularly in terms of seasonality and magnitude, exhibited significant improvement in the modified SWAT-Carbon model (Figure 4a and 4b, Table 2). The inaccuracy of LAI simulation in the original model was attributed to the initiation and end of vegetation dormancy being determined only by a latitude-based daylength threshold. This approach leads to mismatches in the timing of phenological stages in the LAI curve compared to observed data (Figure 4a, 4b, and Figure S1). Based on the widely used processed phenological models (Fu et al., 2020), we incorporated the phenology module into the SWAT-Carbon model, which provides a method for accurately simulating the timing of vegetation growth stages and the runoff simulation. In addition, the highest and lowest simulated LAI values in the original model showed significant underestimation. This is attributed to the inability to meet the default constant value of heat accumulation requirements, owing to low daily temperatures in the upper reach of Jinsha River watershed. In the modified model, we replaced the constant value with a dynamic heat accumulation requirement and optimized vegetation growth parameters, which finally enhanced the simulation accuracy of LAI values and thereby improved runoff simulation. Therefore, we highlight the importance of integrating ~~a~~ the phenology module into hydrological models.

Our study indicated that the modified SWAT-Carbon model improved the simulation of vegetation and runoff. However, some uncertainties from dataset and model persist in the modified model and should be addressed. The meteorological input data used in this study were obtained from a gridded source, which may differ from actual conditions. ~~In addition to vegetation phenology, ecosystem structure, such as species composition is also affected by climate change (Chuine, 2010; Huang et al., 2019), which would substantially impact interactions between vegetation phenology and hydrology processes~~In addition, climate-sensitive ecosystem structures, such as species composition, introduce uncertainties in assessing interactions between vegetation phenology and hydrological processes in the modified SWAT-Carbon model (Chuine, 2010; Huang et al., 2019). ~~Hence~~Therefore~~, more~~ coupling advanced land surface dynamic vegetation models, such as ~~the~~ LPJ-GUESS (Sitch et al., 2003), with hydrological models could ~~be coupled with hydrological models to~~ further improve our understanding of future vegetation dynamics and ~~its~~ their effects on the carbon and water cycles.

4.2 Interaction between Vegetation Phenology and Hydrological Processes

Our results indicated significant improvement in the performance of runoff simulation, particularly during the vegetation greening period (June) and the senescence period (October) (Table 2 and Table S3), which is attributed to the accurate phenology prediction. Vegetation phenology and hydrological processes are closely intertwined through biotic and abiotic pathways (Buermann et al., 2018; Lian et al., 2020). In the upper reaches of Jinsha River watershed, the multiyear mean SOS and EOS occurred in June and October (Figure 2), respectively. During the start and end of the growing season, rapid changes in vegetation physiological properties, such as stomatal conductance and LAI, influence the timing and amount of water resource allocation (Hwang et al., 2023; Zhang et al., 2021).

~~For example~~In addition, the ~~physiological activity of~~ vegetation dynamics and ~~its~~ their impact on the underlying land surface properties ~~of a~~affect watershed ~~affect land surface~~ evapotranspiration (Chen et al., 2022b). To explore the response of ET to vegetation phenology in the upper reaches of Jinsha River watershed, we analyzed the relationship between the phenological variations and sub-basin scale ET using the modified SWAT-Carbon model. Consistent~~In line~~ with previous studies in the Northern Hemisphere, our study revealed a positive correlation between ET and growing season length (Figure 7), potentially attributed to the prolonged period of water movement from the soil to the atmosphere (Geng et al., 2020; Yang et al., 2023). This was further verified by the observation that earlier leaf unfolding and delayed leaf senescence increased spring and autumn ET ~~(Figure S2)~~. ~~Furthermore, v~~Vegetation phenology influences the development and decay of the canopy, altering the water demands of vegetation~~,~~ and ~~contributing to the augmentation of the water~~ affecting the hydrological cycle (Hwang et al., 2018; Lian et al., 2020). However, our study found that both spring and autumn ET increased by ~~a~~ similar magnitudes, with values of 1.58 and 1.62 mm per day, respectively. This finding is inconsistent with the asymmetrical increase reported in previous research (Kim et al., 2018), which ~~could~~ may be attributable to the abundant soil moisture during summer in our study area. This moisture abundance does not impose constraints on vegetation growth and transpiration.

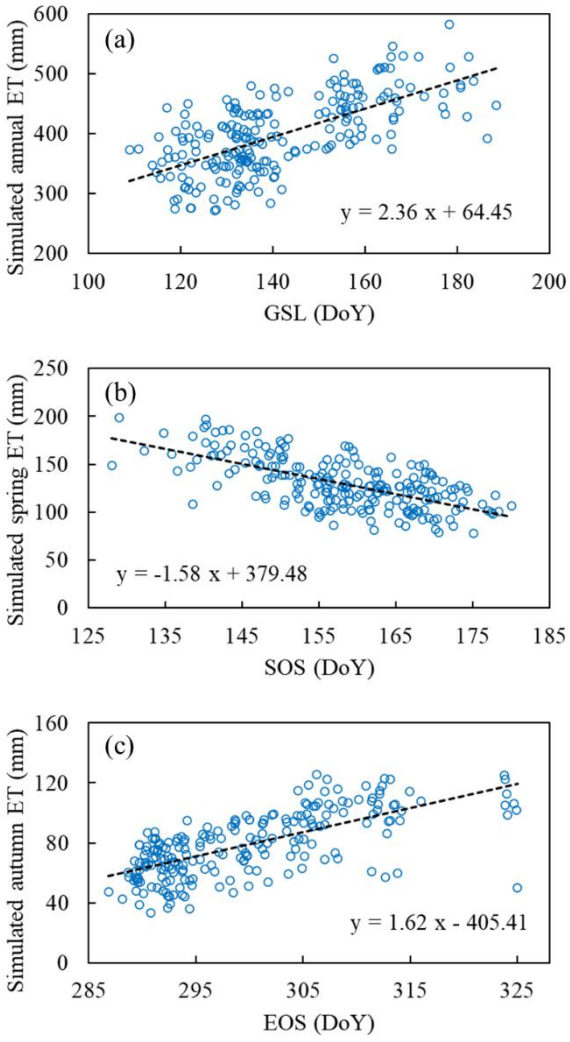

Figure 7: Relationship between the phenological variations and sub-basin scales evapotranspiration (ET) using modified SWAT-Carbon model. GSL, growing season length; SOS, start-of-season; EOS, end-of-season; ET, evapotranspiration.

4.3 Hydrological Response to Future Climate Change and Vegetation Dynamics

We predicted future runoff in the upper reaches of the Jinsha River watershed ~~under~~ and found that the runoff would largely increase under future climate change conditions~~emission scenario~~. Specifically, ~~Under~~ under the SSP5-8.5 scenario, runoff exhibited the most pronounced upward trend, primarily attributed to increased precipitation largely surpassing that of the SSP1-2.6 and SSP2-4.5 scenarios (Figure 6 and Figure S4). In addition to precipitation, the early SOS and delayed EOS under global warming (Figure 5), which were predicted in the upper reaches of Jinsha River watershed, also play an important role in altering the water cycle~~,~~. ~~despite~~ Despite a substantial increase in precipitation under SSP2-4.5 compared to SSP1-2.6, the projected runoff under SSP2-4.5 is marginally smaller than that under SSP1-2.6. This phenomenon ~~can be~~is

likely attributed to the extension of the growing season under global warming, which ~~would~~ significantly increases evapotranspiration under the moderate emission pathway compared to the low emission pathway (Lu et al., 2021; Yang et al., 2023). The increased precipitation under SSP2-4.5 is insufficient to fully counteract the increase in evapotranspiration caused by the prolonged growing season (Figure S4~~3~~).

In this study, future runoff simulation by the original SWAT-Carbon model is smaller than that by the modified model, especially under the high emission scenario, which is also observed in the historical runoff (Figure 4c). The underestimation of historical runoff simulation is attributed to lower baseflow compared to observed data, particularly during the non-rainy season. This discrepancy is potentially influenced by underestimated LAI simulations and unreasonable parameters in the original SWAT-Carbon model (Tang et al., 2022). Vegetation degradation is reported to lead to decreased flow during the dry season (Paiva et al., 2023). In addition, although calibration algorithms enhance the original model's ability to produce accurate runoff simulations, the ~~The~~ unrealistic representation of vegetation phenological processes necessitates remediation through additional ecohydrological processes (Luan et al., 2022; Haas et al., 2022),~~in current hydrological models often requires remediation through additional ecohydrological processes (Luan et al., 2022),~~ thereby compromising the model's fidelity~~ mechanics~~. Therefore, improving the simulation accuracy of vegetation dynamics could enhance the capability of hydrological models to accurately depict ecohydrological processes, especially in the dry season, thereby facilitating more effective water resource conservation strategies under future global warming.~~.~~

5 Conclusions

In summary, our study integrated a process-based vegetation phenology module into the SWAT-Carbon model, substantially improving the simulation of vegetation dynamics and hydrological processes in the upper reaches of the Jinsha River watershed. The runoff is predicted to increase over 2030-2100 under different future emission scenarios, primarily due to greater precipitation outweighing the increase in evapotranspiration induced by the prolonged growing season. Our study highlights the importance of integrating phenological shifts into hydrological models. In the future, it will be crucial to consider and couple plant functional types ~~into~~ with hydrological models to further enhance the performance of ecohydrological process simulations. Furthermore, the phenology module should be incorporated into other hydrological models and applied in various watersheds to enhance our understanding of ecohydrological processes and to support future water resources management under climate change conditions.

Data availability

Datasets for driving and evaluating the phenology models and the SWAT-Carbon model are available from the sources listed in Table 1.

Author contributions

Conceptualization: YF; Data curation: NW, JZ; Formal Analysis: ML, SC; Funding acquisition: YF, FH; Methodology: ML, SC, YX, ZW; Software: ML, SC; Supervision: YF; Validation: SC; Visualization: ML, JZ; Writing – original draft: ML; Writing – review & editing: SC, FH, NW, ZW, YX, JZ, YZ, YF.

Competing interests

The authors declare that they have no known competing financial interests or personal relationships that could have appeared to influence the work reported in this paper.

Acknowledgments

This study was supported by the National Science Fund for Distinguished Young Scholars (No.42025101), the Joint Fund for Regional Innovation and Development of the National Natural Science Foundation of China (~~Grant~~ No. U21A2039)~~, the National Science Fund for Distinguished Young Scholars (42025101)~~, and the National Natural Science Foundation of China (No.42330515).

References

Abbaspour K. C.: SWAT Calibration and Uncertainty Programs, A User Manual, 2008.

Arnold J. G., Srinivasan R., Muttiah R. S., and Williams J. R.: Large Area Hydrologic Modeling and Assessment Part I: Model Development, J. Am. Water Resour. As., 34, 73–89, https://doi.org/10.1111/j.1752-1688.1998.tb05961.x, 1998.

Arnold J. G., Moriasi D. N., Gassman P., Abbaspour K. C., White M. J., Srinivasan R., Santhi C., Harmel R. D., Van Griensven A., Van Liew M. W., Kannan N., and Jha M. K.: SWAT: Model Use, Calibration, and Validation, T. ASABE, 55, 1491–1508, https://doi.org/10.13031/2013.42256, 2012.

Bhatta, B., Shrestha, S., Shrestha, P. K., and Talchabhadel, R.: Evaluation and application of a SWAT model to assess the climate change impact on the hydrology of the Himalayan River Basin, CATENA, 181, 104082, https://doi.org/10.1016/j.catena.2019.104082, 2019.

Bonan, G. B.: Forests and Climate Change: Forcings, Feedbacks, and the Climate Benefits of Forests, Science, 320, 1444–1449, https://doi.org/10.1126/science.1155121, 2008.

Buermann W., Forkel M., O'Sullivan M., Sitch S., Friedlingstein P., Haverd V., Jain A. K., Kato E., Kautz M., Lienert S., Lombardozzi D., Nabel J. E. M. S., Tian H., Wiltshire A. J., Zhu D., Smith W. K., and Richardson A. D.: Widespread seasonal compensation effects of spring warming on northern plant productivity, Nature, 562, 110–114, https://doi.org/10.1038/s41586-018-0555-7, 2018.

Chen S., Fu Y. H., Geng X., Hao Z., Tang J., Zhang X., Xu Z., and Hao F.: Influences of Shifted Vegetation Phenology on Runoff Across a Hydroclimatic Gradient, Front. Plant Sci., 12, https://doi.org/10.3389/fpls.2021.802664， 2022a.

Chen S., Fu Y. H., Hao F., Li X., Zhou S., Liu C., and Tang J.: Vegetation phenology and its ecohydrological implications from individual to global scales, Geography and Sustainability, 3, 334–338, https://doi.org/10.1016/j.geosus.2022.10.002, 2022b.

Chen S., Fu Y. H., Wu Z., Hao F., Hao Z., Guo Y., Geng X., Li X., Zhang X., Tang J., Singh V. P., and Zhang X.: Informing the SWAT model with remote sensing detected vegetation phenology for improved modeling of ecohydrological processes, J. Hydrol., 616, 128817, https://doi.org/10.1016/j.jhydrol.2022.128817, 2023.

Chuine, I.: A Unified Model for Budburst of Trees, J. Theor. Biol., 207, 337–347, https://doi.org/10.1006/jtbi.2000.2178, 2000.

Chuine, I.: Why does phenology drive species distribution?, Phil. Trans. R. Soc. B., 365, 3149–3160, https://doi.org/10.1098/rstb.2010.0142, 2010.

Creed, I. F., Hwang, T., Lutz, B., and Way, D.: Climate warming causes intensification of the hydrological cycle, resulting in changes to the vernal and autumnal windows in a northern temperate forest, Hydrol. Process., 29, 3519–3534, https://doi.org/10.1002/hyp.10450, 2015.

Cui T., Martz L., and Guo X.: Grassland Phenology Response to Drought in the Canadian Prairies, Remote Sens., 9, 1258, https://doi.org/10.3390/rs9121258, 2017.

Delpierre N., Dufrêne E., Soudani K., Ulrich E., Cecchini S., Boé J., and François C.: Modelling interannual and spatial variability of leaf senescence for three deciduous tree species in France, Agr. Forest Meteorol., 149, 938–948, https://doi.org/10.1016/j.agrformet.2008.11.014, 2009.

Fu, Y., Li, X., Zhou, X., Geng, X., Guo, Y., and Zhang, Y.: Progress in plant phenology modeling under global climate change, Sci. China Earth Sci., 63, 1237–1247, https://doi.org/10.1007/s11430-019-9622-2, 2020.

Fu Y. H., Campioli M., Demarée G., Deckmyn A., Hamdi R., Janssens I. A., and Deckmyn G.: Bayesian calibration of the Unified budburst model in six temperate tree species, Int. J. Biometeorol., 56, 153–164, https://doi.org/10.1007/s00484-011-0408-7, 2012.

Fu, Y. H., Piao, S., Op De Beeck, M., Cong, N., Zhao, H., Zhang, Y., Menzel, A., and Janssens, I. A.: Recent spring phenology shifts in western Central Europe based on multiscale observations, Global Ecol. Biogeogr., 23, 1255–1263, https://doi.org/10.1111/geb.12210, 2014.

Fu, Y. H., Zhao, H., Piao, S., Peaucelle, M., Peng, S., Zhou, G., Ciais, P., Huang, M., Menzel, A., Peñuelas, J., Song, Y., Vitasse, Y., Zeng, Z., and Janssens, I. A.: Declining global warming effects on the phenology of spring leaf unfolding, Nature, 526, 104–107, https://doi.org/10.1038/nature15402, 2015.

Fu, Y. H., Piao, S., Delpierre, N., Hao, F., Hänninen, H., Liu, Y., Sun, W., Janssens, I. A., and Campioli, M.: Larger temperature response of autumn leaf senescence than spring leaf-out phenology, Glob. Change Biol., 24, 2159–2168, https://doi.org/10.1111/gcb.14021, 2018.

Fu, Y. H., Zhou, X., Li, X., Zhang, Y., Geng, X., Hao, F., Zhang, X., Hanninen, H., Guo, Y., and De Boeck, H. J.: Decreasing control of precipitation on grassland spring phenology in temperate China, Global Ecol. Biogeogr., 30, 490–499, https://doi.org/10.1111/geb.13234, 2021.

Gaertner, B. A., Zegre, N., Warner, T., Fernandez, R., He, Y., and Merriam, E. R.: Climate, forest growing season, and evapotranspiration changes in the central Appalachian Mountains, USA, Sci. Total Environ., 650, 1371–1381, https://doi.org/10.1016/j.scitotenv.2018.09.129, 2019.

Garonna I., de Jong R., and Schaepman M. E.: Variability and evolution of global land surface phenology over the past three decades (1982–2012), Glob. Change Biol., 22, 1456–1468, https://doi.org/10.1111/gcb.13168, 2016.

Ge, Q., Wang, H., Rutishauser, T., and Dai, J.: Phenological response to climate change in China: a meta-analysis, Glob. Change Biol., 21, 265–274, https://doi.org/10.1111/gcb.12648, 2015.

Geng, X., Zhou, X., Yin, G., Hao, F., Zhang, X., Hao, Z., Singh, V. P., and Fu, Y. H.: Extended growing season reduced river runoff in Luanhe River basin, J. Hydrol., 582, 124538, https://doi.org/10.1016/j.jhydrol.2019.124538, 2020.

Gudmundsson L., Bremnes J. B., Haugen J. E., and Engen-Skaugen T.: Technical Note: Downscaling RCM precipitation to the station scale using statistical transformations – a comparison of methods, Hydrol. Earth Syst. Sci., 16, 3383–3390, https://doi.org/10.5194/hess-16-3383-2012, 2012.

He, J., Yang, K., Tang, W., Lu, H., Qin, J., Chen, Y., and Li, X.: The first high-resolution meteorological forcing dataset for land process studies over China, Sci. Data, 7, 25, https://doi.org/10.1038/s41597-020-0369-y, 2020.

He, K., Chen, X., Zhou, J., Zhao, D., and Yu, X.: Compound successive dry-hot and wet extremes in China with global warming and urbanization, J. Hydrol., 636, 131332, https://doi.org/10.1016/j.jhydrol.2024.131332, 2024.

Haas, H., Kalin, L., and Srivastava, P.: Improved forest dynamics leads to better hydrological predictions in watershed modeling, Sci. Total Environ., 821, 153180, https://doi.org/10.1016/j.scitotenv.2022.153180, 2022.

Huang, M., Piao, S., Ciais, P., Peñuelas, J., Wang, X., Keenan, T. F., Peng, S., Berry, J. A., Wang, K., Mao, J., Alkama, R., Cescatti, A., Cuntz, M., De Deurwaerder, H., Gao, M., He, Y., Liu, Y., Luo, Y., Myneni, R. B., Niu, S., Shi, X., Yuan, W., Verbeeck, H., Wang, T., Wu, J., and Janssens, I. A.: Air temperature optima of vegetation productivity across global biomes, Nat. Ecol. Evol., 3, 772–779, https://doi.org/10.1038/s41559-019-0838-x, 2019.

Hwang, T., Band, L. E., Miniat, C. F., Song, C., Bolstad, P. V., Vose, J. M., and Love, J. P.: Divergent phenological response to hydroclimate variability in forested mountain watersheds, Glob. Change Biol., 20, 2580–2595, https://doi.org/10.1111/gcb.12556, 2014.

Hwang, T., Martin, K. L., Vose, J. M., Wear, D., Miles, B., Kim, Y., and Band, L. E.: Nonstationary Hydrologic Behavior in Forested Watersheds Is Mediated by Climate-Induced Changes in Growing Season Length and Subsequent Vegetation Growth, Water Resour. Res., 54, 5359–5375, https://doi.org/10.1029/2017WR022279, 2018.

Hwang T., Band L. E., Oishi A. C., and Kang H.: Greenup Variability Impact on Seasonal Streamflow and Soil Moisture Dynamics in Humid, Temperate Forests, Water Resour. Res., 59, e2022WR034125, https://doi.org/10.1029/2022WR034125, 2023.

IPCC,2021: Climate Change 2021: The Physical Science Basis: Working Group I Contribution to the Sixth Assessment Report of the Intergovernmental Panel on Climate Change, Cambridge University Press, Cambridge, United Kingdom and New York, NY, USA, https://doi.org/10.1017/9781009157896, 2021.

Jiang, Q., Yuan, Z., Yin, J., Yao, M., Qin, T., Lü, X., and Wu, G.: Response of vegetation phenology to climate factors in the source region of the Yangtze and Yellow Rivers, J. Plant Ecol., 17, rtae046, https://doi.org/10.1093/jpe/rtae046, 2024.

Kim, J. H., Hwang, T., Yang, Y., Schaaf, C. L., Boose, E., and Munger, J. W.: Warming-Induced Earlier Greenup Leads to Reduced Stream Discharge in a Temperate Mixed Forest Catchment, J. Geophys. Res. Biogeo., 123, 1960–1975, https://doi.org/10.1029/2018JG004438, 2018.

Li, X., Long, D., Scanlon, B. R., Mann, M. E., Li, X., Tian, F., Sun, Z., and Wang, G.: Climate change threatens terrestrial water storage over the Tibetan Plateau, Nat. Clim. Change, 1–7, https://doi.org/10.1038/s41558-022-01443-0, 2022.

Lian, X., Piao, S., Li, L. Z. X., Li, Y., Huntingford, C., Ciais, P., Cescatti, A., Janssens, I. A., Peñuelas, J., Buermann, W., Chen, A., Li, X., Myneni, R. B., Wang, X., Wang, Y., Yang, Y., Zeng, Z., Zhang, Y., and McVicar, T. R.: Summer soil drying exacerbated by earlier spring greening of northern vegetation, Sci. Adv., 6, eaax0255, https://doi.org/10.1126/sciadv.aax0255, 2020.

Lu J., Wang G., Li S., Feng A., Zhan M., Jiang T., Su B., and Wang Y.: Projected Land Evaporation and Its Response to Vegetation Greening Over China Under Multiple Scenarios in the CMIP6 Models, J. Geophys. Res. Biogeo., 126, e2021JG006327, https://doi.org/10.1029/2021JG006327, 2021.

Luan, J., Miao, P., Tian, X., Li, X., Ma, N., Abrar Faiz, M., Xu, Z., and Zhang, Y.: Estimating hydrological consequences of vegetation greening, J. Hydrol., 611, 128018, https://doi.org/10.1016/j.jhydrol.2022.128018, 2022.

Ma, T., Duan, Z., Li, R., and Song, X.: Enhancing SWAT with remotely sensed LAI for improved modelling of ecohydrological process in subtropics, J. Hydrol., 570, 802–815, https://doi.org/10.1016/j.jhydrol.2019.01.024, 2019.

Moriasi, D. N., Arnold, J. G., Liew, M. W. V., Bingner, R. L., Harmel, R. D., and Veith, T. L.: Model Evaluation Guidelines for Systematic Quantification of Accuracy in Watershed Simulations, T. ASABE, 50, 885–900, https://doi.org/10.13031/2013.23153, 2007.

Mukundan, R., Gelda, R. K., Moknatian, M., Zhang, X., and Steenhuis, T. S.: Watershed scale modeling of Dissolved organic carbon export from variable source areas, J. Hydrol., 625, 130052, https://doi.org/10.1016/j.jhydrol.2023.130052, 2023.

Neitsch S. L., Arnold J. G., Kiniry J. R., and Williams J. R.: Soil and water assessment tool theoretical documentation version 2009, 2011.

Paiva K., Rau P., Montesinos C., Lavado-Casimiro W., Bourrel L., and Frappart F.: Hydrological Response Assessment of Land Cover Change in a Peruvian Amazonian Basin Impacted by Deforestation Using the SWAT Model, Remote Sens., 15, 5774, https://doi.org/10.3390/rs15245774, 2023.

Peñuelas J., Filella I., Zhang X., Llorens L., Ogaya R., Lloret F., Comas P., Estiarte M., and Terradas J.: Complex spatiotemporal phenological shifts as a response to rainfall changes, New Phytol., 161, 837–846, https://doi.org/10.1111/j.1469-8137.2004.01003.x, 2004.

Piao, S., Tan, J., Chen, A., Fu, Y. H., Ciais, P., Liu, Q., Janssens, I. A., Vicca, S., Zeng, Z., Jeong, S.-J., Li, Y., Myneni, R. B., Peng, S., Shen, M., and Peñuelas, J.: Leaf onset in the northern hemisphere triggered by daytime temperature, Nat. Commun., 6, 6911, https://doi.org/10.1038/ncomms7911, 2015.

Piao, S., Liu, Q., Chen, A., Janssens, I. A., Fu, Y., Dai, J., Liu, L., Lian, X., Shen, M., and Zhu, X.: Plant phenology and global climate change: Current progresses and challenges, Glob. Change Biol., 25, 1922–1940, https://doi.org/10.1111/gcb.14619, 2019.

Roberts, A. M. I., Tansey, C., Smithers, R. J., and Phillimore, A. B.: Predicting a change in the order of spring phenology in temperate forests, Glob. Change Biol., 21, 2603–2611, https://doi.org/10.1111/gcb.12896, 2015.

Shen, M., Wang, S., Jiang, N., Sun, J., Cao, R., Ling, X., Fang, B., Zhang, L., Zhang, L., Xu, X., Lv, W., Li, B., Sun, Q., Meng, F., Jiang, Y., Dorji, T., Fu, Y., Iler, A., Vitasse, Y., Steltzer, H., Ji, Z., Zhao, W., Piao, S., and Fu, B.: Plant phenology changes and drivers on the Qinghai–Tibetan Plateau, Nat. Rev. Earth Environ., 3, 633–651, https://doi.org/10.1038/s43017-022-00317-5, 2022.

Sitch S., Smith B., Prentice I. C., Arneth A., Bondeau A., Cramer W., Kaplan J. O., Levis S., Lucht W., Sykes M. T., Thonicke K., and Venevsky S.: Evaluation of ecosystem dynamics, plant geography and terrestrial carbon cycling in the LPJ dynamic global vegetation model, Glob. Change Biol., 9, 161–185, https://doi.org/10.1046/j.1365-2486.2003.00569.x, 2003.

Stevens B. and Bony S.: What Are Climate Models Missing?, Science, 340, 1053–1054, https://doi.org/10.1126/science.1237554, 2013.

Strauch M. and Volk M.: SWAT plant growth modification for improved modeling of perennial vegetation in the tropics, Ecol. Model., 269, 98–112, https://doi.org/10.1016/j.ecolmodel.2013.08.013, 2013.

Tang Z., Zhou Z., Wang D., Luo F., Bai J., and Fu Y.: Impact of vegetation restoration on ecosystem services in the Loess plateau, a case study in the Jinghe Watershed, China, Ecol. Indic., 142, 109183, https://doi.org/10.1016/j.ecolind.2022.109183, 2022.

Thrasher B., Maurer E. P., McKellar C., and Duffy P. B.: Technical Note: Bias correcting climate model simulated daily temperature extremes with quantile mapping, Hydrol. Earth Syst. Sci., 16, 3309–3314, https://doi.org/10.5194/hess-16-3309-2012, 2012.

Tian, P., Lu, H., Feng, W., Guan, Y., and Xue, Y.: Large decrease in streamflow and sediment load of Qinghai–Tibetan Plateau driven by future climate change: A case study in Lhasa River Basin, CATENA, 187, 104340, https://doi.org/10.1016/j.catena.2019.104340, 2020.

Vitasse, Y., Baumgarten, F., Zohner, C. M., Rutishauser, T., Pietragalla, B., Gehrig, R., Dai, J., Wang, H., Aono, Y., and Sparks, T. H.: The great acceleration of plant phenological shifts, Nat. Clim. Change, 12, 300–302, https://doi.org/10.1038/s41558-022-01283-y, 2022.

Wang K., Onodera S., Saito M., Shimizu Y., and Iwata T.: Effects of forest growth in different vegetation communities on forest catchment water balance, Sci. Total Environ., 809, 151159, https://doi.org/10.1016/j.scitotenv.2021.151159, 2022.

Wilcke R. A. I., Mendlik T., and Gobiet A.: Multi-variable error correction of regional climate models, Climatic Change, 120, 871–887, https://doi.org/10.1007/s10584-013-0845-x, 2013.

Wu Y., Fang H., Huang L., and Ouyang W.: Changing runoff due to temperature and precipitation variations in the dammed Jinsha River, J. Hydrol., 582, 124500, https://doi.org/10.1016/j.jhydrol.2019.124500, 2020.

Wu, Z., Chen, S., De Boeck, H. J., Stenseth, N. C., Tang, J., Vitasse, Y., Wang, S., Zohner, C., and Fu, Y. H.: Atmospheric brightening counteracts warming-induced delays in autumn phenology of temperate trees in Europe, Global Ecol. Biogeogr., 30, 2477–2487, https://doi.org/10.1111/geb.13404, 2021.

Wu Z., Fu Y. H., Crowther T. W., Wang S., Gong Y., Zhang J., Zhao Y.-P., Janssens I., Penuelas J., and Zohner C. M.: Poleward shifts in the maximum of spring phenological responsiveness of Ginkgo biloba to temperature in China, New Phytol., 240, 1421–1432, https://doi.org/10.1111/nph.19229, 2023.

Yang X., Mustard J. F., Tang J., and Xu H.: Regional-scale phenology modeling based on meteorological records and remote sensing observations, J. Geophys. Res. Biogeo., 117, https://doi.org/10.1029/2012JG001977, 2012.

Yang Y., Roderick M. L., Guo H., Miralles D. G., Zhang L., Fatichi S., Luo X., Zhang Y., McVicar T. R., Tu Z., Keenan T. F., Fisher J. B., Gan R., Zhang X., Piao S., Zhang B., and Yang D.: Evapotranspiration on a greening Earth, Nat. Rev. Earth Environ., https://doi.org/10.1038/s43017-023-00464-3, 2023.

Zhang, C., Sun, F., Sharma, S., Zeng, P., Mejia, A., Lyu, Y., Gao, J., Zhou, R., and Che, Y.: Projecting multi-attribute flood regime changes for the Yangtze River basin, J. Hydrol., 617, 128846, https://doi.org/10.1016/j.jhydrol.2022.128846, 2023.

Zhang H., Wang B., Liu D. L., Zhang M., Leslie L. M., and Yu Q.: Using an improved SWAT model to simulate hydrological responses to land use change: A case study of a catchment in tropical Australia, J. Hydrol., 585, 124822, https://doi.org/10.1016/j.jhydrol.2020.124822, 2020.

Zhang, X., Izaurralde, R. C., Arnold, J. G., Williams, J. R., and Srinivasan, R.: Modifying the Soil and Water Assessment Tool to simulate cropland carbon flux: Model development and initial evaluation, Sci. Total Environ., 463–464, 810–822, https://doi.org/10.1016/j.scitotenv.2013.06.056, 2013.

Zhang X., Zhang Y., Ma N., Kong D., Tian J., Shao X., and Tang Q.: Greening-induced increase in evapotranspiration over Eurasia offset by CO_2-induced vegetational stomatal closure, Environ. Res. Lett., 16, 124008, https://doi.org/10.1088/1748-9326/ac3532, 2021.

Zhang Y., Chiew F. H. S., Zhang L., and Li H.: Use of Remotely Sensed Actual Evapotranspiration to Improve Rainfall–Runoff Modeling in Southeast Australia, J. Hydrometeorol., 10, 969–980, https://doi.org/10.1175/2009JHM1061.1, 2009.

Zhao J., Zhang H., Zhang Z., Guo X., Li X., and Chen C.: Spatial and Temporal Changes in Vegetation Phenology at Middle and High Latitudes of the Northern Hemisphere over the Past Three Decades, Remote Sens., 7, 10973–10995, https://doi.org/10.3390/rs70810973, 2015.

Zhou S., Yu B., Lintner B. R., Findell K. L., and Zhang Y.: Projected increase in global runoff dominated by land surface changes, Nat. Clim. Change, 1–8, https://doi.org/10.1038/s41558-023-01659-8, 2023.